ORIGINAL ARTICLE

Effect of post weld heat treatment on the microstructure and mechanical properties of a gas-tungsten-arc-welded 304 stainless steel

Ahmed Kellai[1] · Sami Kahla[1] · Said Dehimi[1] · Liamine Kaba[1] · Zoheir Boutaghou[1]

Abstract

In this work, the microstructural evolution and mechanical properties of 304 austenitic stainless steel welds produced by GTAW process were examined after post weld heat treatment (PWHT). Thermal treatment was carried out at different temperatures ranging from 450 to 1050 °C. The optical microscope and scanning electron microscope were used to study the microstructure and fracture surface of the welded joints. X-ray diffraction (XRD) and energy-dispersive spectroscopy (EDS) techniques were used to investigate the possible formation of intermetallic phases as σ or chromium carbide. Based on the results, no σ phase or chromium carbide precipitation was found. Also, the mechanical behavior of the joint was evaluated by tensile and microhardness tests. The microstructure of the 304 stainless steel was found to consist of equiaxed austenite grains (γ) of various sizes limited by grain boundaries and twin crystals with small amount of delta ferrite (δ) in grain boundaries. The microstructure of the weld metal was austenite with dendritic structure containing skeletal delta-ferrite. The skeletal type delta-ferrite changed from columnar + equiaxed to cellular type by progression during heat treatment. The base metal (BM) and heat affected zone (HAZ) grain size decreased with increasing heat treatment temperature. Therefore, the mechanical testing results were appropriately correlated with the microstructure analysis. Tensile testing analysis showed that the highest tensile strength value was recorded for the as-welded specimen. On the other hand, the PWHT temperature has less effect on the tensile strengths but improves the elongation of the weldments. The micro-hardness for all the weld zones WZs exhibited lower values than that of the base metal BM and the heat affected zone HAZ. The latter presents similar micro-hardness values for all samples and slightly higher than that of the BM except for the weld heat treated at 850 °C, which attained high micro-hardness values. The weldment solution heat treated at 1050 °C shows the best and stable micro-hardness profile similar to that of the as-weld specimen but with higher values in the weld zone.

Keywords Austenitic 304 stainless steels · Gas tungsten arc welding (GTAW) · Post weld heat treatment (PWHT) · Microstructure and mechanical properties

✉ Ahmed Kellai
    a.kellai@crti.dz; kellai.a.a@gmail.com

    Sami Kahla
    samikahla40@yahoo.com

    Said Dehimi
    s.dehimi@crti.dz

    Liamine Kaba
    l.kaba@crti.dz

    Zoheir Boutaghou
    z.boutaghou@crti.dz

[1] Research Center in Industrial Technologies, CRTI, P.O. Box 64, Cheraga 16014, Algiers, Algeria

1 Introduction

Stainless steels are alloys of iron, chromium, possibly nickel, and other alloying elements. And depending on their chromium content and the metallurgical treatments they undergo, they may exhibit a wide range of properties. Austenitic stainless steels constitute an interesting class of the main groups of stainless steels because of their excellent mechanical properties (toughness and ductility), corrosion resistance, at low and high temperature, and weldability [1–4]. This is particularly so for austenitic stainless steel 304, which has become indispensable for many applications and more so in the gas and petroleum industries. However, there are various phenomena during the welding of this kind of steels that can

affect them, namely, (i) distribution of alloying elements; (ii) precipitation of intermetallic phases, and (iii) segregation during solidification [5–7].

It is well known that in the case where solidification occurs under equilibrium conditions, the microstructure of the austenitic stainless steel is mostly composed of austenite (FCC). However, if the solidification condition is non-equilibrium as in the case of welding with a high cooling rate, a certain amount of metastable δ-ferrite will inevitably remain due to incomplete transformation of ferrite-to-austenite [8]. Normally, the δ-ferrite content in the weld metal of the austenitic stainless steel varies from 2 to 10%. To avoid the phenomenon of hot cracking during weld solidification, a small amount of δ-ferrite is essential [9]. On the other hand, when the welds are intended for service at high temperatures (> 500 °C), a high ferrite content is not recommended, because at high temperature most intermetallic phases are formed from metastable ferrite, which will influence the mechanical properties [10].

During the thermal cycle of welding process, when stainless steels are exposed to critical temperature in the range 600–1050 °C, where intermetallic phases occur particularly in the heat affected zone (HAZ) such as σ, χ, and Cr-Fe rich carbides, this often leads to bad metallurgical changes that weaken the mechanical properties [7, 8, 11]. The precipitation of Cr-Fe rich carbides at the grain boundaries or phase boundaries leads of Cr-deficient in the heat affected zone resulting in brittleness, welding decay, and reduced corrosion resistance [12–14].

A suitable post-heat treatment can homogenize the microstructure of the welded material and control the formation of intermetallic phases resulting in improved mechanical properties [14]. The conservation of intermetallic phases during hyperquenching in the solution heat treatment at 1050 °C ensured by the presence of molybdenum [15]. A short-time heat treatment of one hour indicates that at temperatures in the range 600–760 °C there are no precipitates in the fusion zone but the residual stresses will be escaped. However, at temperatures between 870 and 920 °C there is sigma phase precipitation as detected by EDS, which reduces the impact toughness [16]. Heat treatment at 1050 °C for 1 h recovers the properties of the base material, whereas a treatment at 800 °C for 10 h reduces the yield strength and increases the tensile strength [17]. The ferrite content decreases with increasing heat treatment temperature from 600 up to 900 °C for 2 h with formation of carbide and sigma phase detect by EDS [18].

Gas tungsten arc welding (GTAW) is a widely used technique for welding stainless steel pipes. This technique causes microstructural changes and residual stresses resulting in poor mechanical properties and low corrosion resistance in aggressive environments. The main objective is to make a correlation between the changes in the microstructure during aging treatment and the mechanical properties of the welded

joint in order to obtain the optimum PWHT temperature for reducing the residual stress in the weld and ensure a strong and consistent fabrication.

2 Materials and methods

The austenitic stainless steel used in this study was AISI 304 in the form of pipe of 203.2 mm diameter and 3.75 mm thickness. The manual electric arc welding process GTAW was performed using ER308Si (AWS: A5.9) as a filler metal. It is widely used in industry, particularly the oil industry, designed for welding austenitic stainless steels. This type of filler metal contains more molybdenum and silicon than the base metal. This, together with their high nickel content and additions of copper, gives them very good resistance to intergranular corrosion and chloride-induced stress corrosion. Otherwise, the higher silicon content improves wetting of the weld metal and potentially higher travel speeds compared to standard 308L products. The chemical compositions of the materials used are shown in Table 1. To evaluate the microstructures and mechanical properties, changes after post heat treatment, several treatments were performed from 450, 650, 850, and 1050 °C, while maintaining these temperatures for 1 h using furnace of branch (Nabertherm MORE THAN HEAT-30–3000 °C, Germany), the specimens were then quenched in water. The welding parameters used in this study are presented in Table 2.

Samples intended for metallographic observations taken from sections transverse to the welding direction of heat-treated welded joints were prepared using conventional techniques for mechanical polishing, followed by 0.5 µm alumina powder and water polish for the purpose of obtaining a mirror state. Then, the specimens were subjected to electrolytic etching in sulfuric acid solution (H_2SO_4 (5%)) at 4 V for 50 s. The microstructural evaluation of the weld joint for the different zones, namely, base metal (BM), heat affected zone (HAZ) and weld zone (WZ), was carried out before and after the PWHT using an optical and scanning electron microscope analysis. These are a light microscope (Nikon Eclipse LV100ND) and a ZEISS.EVO-MA 25 type equipped with microanalysis system (EDS), respectively. The grain size and phase ratio were measured with the help of image J software.

The X-ray diffraction (XRD) technique with 2θ scanning was used to evaluate the structure and phases present in the BM and WZ. The diffractometer used was a BRUKER D2 PHASER 2G mark equipped with a copper (Cu) anticathode delivering an X-ray wavelength of 1.5406 nm, an acquisition step of 0.02°, a voltage $V = 30$ kV and an intensity $I = 10$ mA.

Table 1 Chemical composition of base metal and filler wire

Chemical composition (wt%)												
Material	C	Mn	Si	S	P	Cr	Ni	Mo	Co	Nb	Cu	Fe
Base metal AISI 304	0.05	2.03	0.68	-	0.04	18.09	8.15	-	0.21	-	0.11	Bal
Filler wire ER308Si	0.02	1.78	1.07	0.03	0.04	19.38	9.33	0.1	0.18	0.03	0.22	Bal

Table 2 GTAW welding parameters

Wire diameter (mm)	Welding current (A)	Welding voltage (V)	Welding speed (mm/mn)	Welding energy (kj/mm)	Inter-pass temperature (°C)	Shielding gas (%)	Flow rate (l/min)	Backing flow (l/min)
2.4	75–85	10–12	70–100	0.612–0.642	150	Ar99.999	12	10

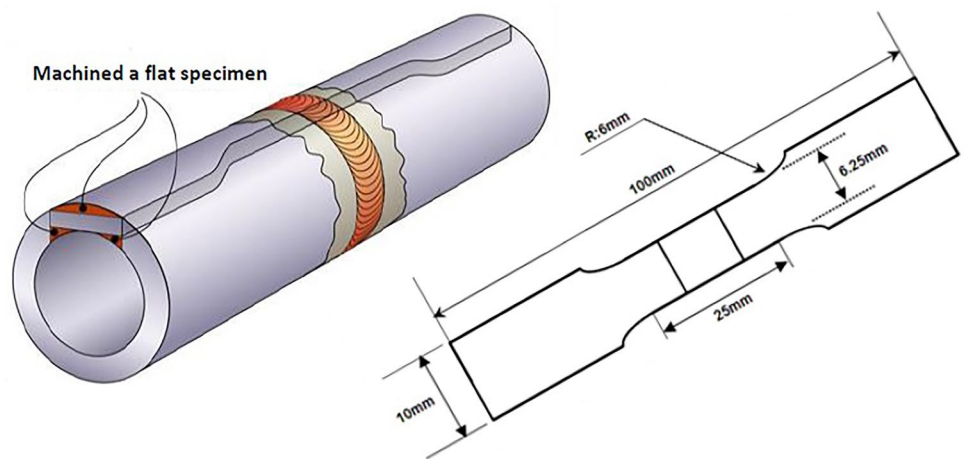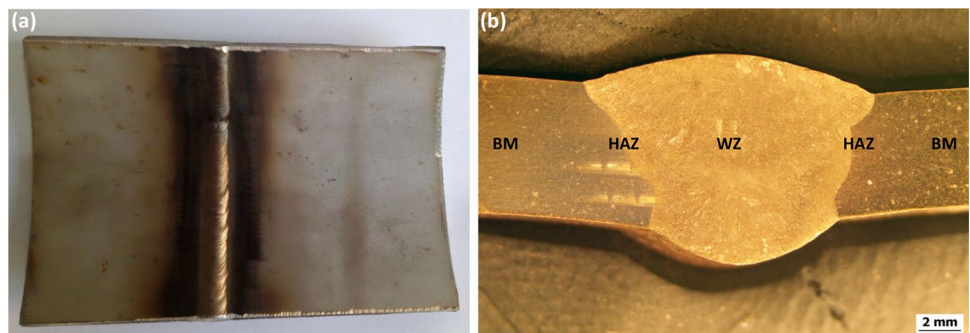**Fig. 1** Dimensions of the tensile test specimen [19]

Fig. 2 Weld joint: (**a**) visual appearance, (**b**) optical macrograph

Mechanical behavior was mainly evaluated by tensile test and micro-hardness profiles. The tensile test was performed at room temperature using an MTS Criterion Model 45 hydraulic test machine. Depending on the thickness of the welded pipe, the tensile test was conducted on sub-sized specimens machined according to ASTM E8-04 standard (Fig. 1) [19]. Micro-hardness distributions across welds were assessed using a Wilson VH3300 automatic hardness testing system with a 200-g loading force and a dwell time of 15 s.

3 Results and discussion

3.1 Macro-examination

Figure 2a shows the visual appearance of the weld joint; there is a good weld with a regular width along the joint without any defect, which shows the importance of the welding process, welding parameters, the qualification of the welder, and finally the good weldability of austenitic stainless steel. Figure 2b presents the different zones constituting a weldment, which are as follows: the base metal (BM), the weld zone (WZ), and the heat affected zone (HAZ).

3.2 Microstructure examination

Figure 3 shows the microstructure of the AISI 304 austenitic stainless steel base metal, consisting of equiaxed (coaxial) austenite grains of various sizes limited by grain boundaries. Twin crystals can be observed in the austenitic matrix (γ) with small amount of delta ferrite (δ) in grain boundaries. No carbide precipitate in the microstructure was found due
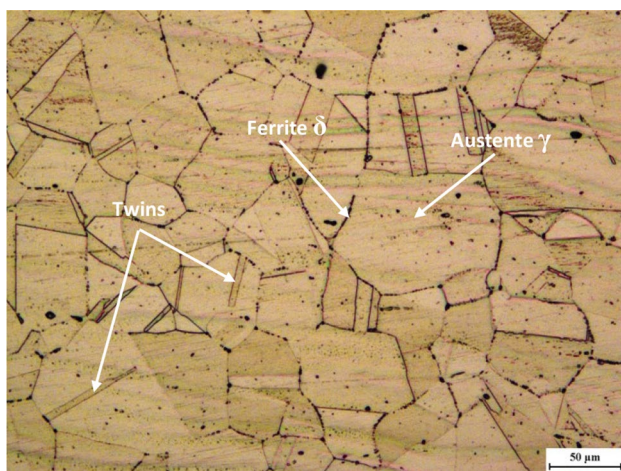
to an appropriate annealing treatment after cold rolling [12, 13, 20, 21].

The temperature reached for 304 austenitic stainless steel welds can be predicted from the pseudo binary phase diagram of Fe–Cr–Ni (Fig. 4). The temperature in the weld zone exceeds 1450 °C. On other hand, the heat affected zone HAZ has reached the temperature range of 550–1200 °C. The solidification microstructures are different for different cooling rates. During cooling of 304, the temperature that δ-ferrite begins to nucleate from liquid decreases with the increase of cooling rate. The cooling rate for quenched welds of the same thicknesses, same grades after PWHT at different temperatures depends on the temperature difference between the weldment and the cooling medium; the greater the difference, the faster the cooling [22, 23]. Several researchers have simulated the cooling rate during GTA welding and shown that the rate varies between 1.2 and 1.5 °C/s. For heat treated welds water-quenched, the cooling rate depends on the temperature gradient, so as the temperature increases, for 450 to 1050 °C, the cooling rate increases. The cooling rate is estimated to be 200 to 600 °C/s [22–25].

The microstructures of base metal BM, fusion boundary, and heat-affected zone HAZ for all specimens, as-welded and heat-treated at 450, 650, 850, and 1050 °C for 1 h, are presented in the optical micrographs of Fig. 5. Following the effect of the welding heat input, the fusion zone of the as-welded is characterized by the rolling structure transforming into dendritic-like grains. The austenite grain size of
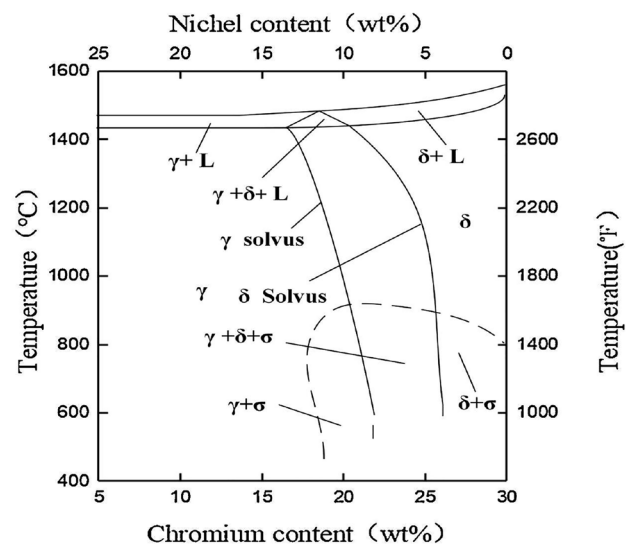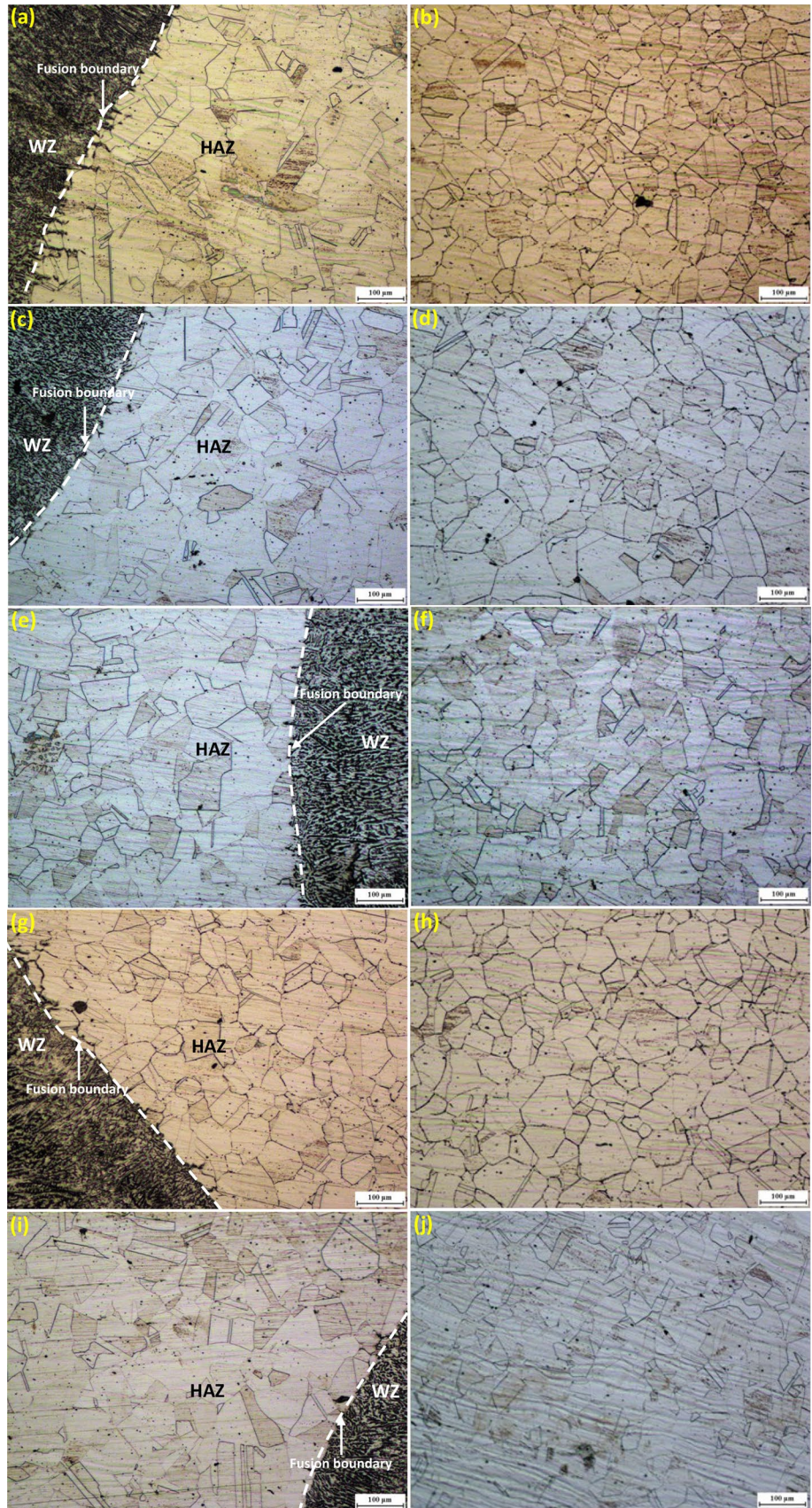

Fig. 3 Optical micrograph of 304 austenitic stainless steel base metal

Fig. 4 Pseudo binary phase diagram of Fe–Cr–Ni for 304 austenitic stainless steel [22, 24]

Fig. 5 Optical micrographs in the fusion boundary and base metal of weldments: **a**, **b** as-welded, **c**, **d** PWHT at 450 °C, **e**, **f** PWHT at 650 °C, **g**, **h** PWHT at 850 °C, **i**, **j** PWHT at 1050 °C
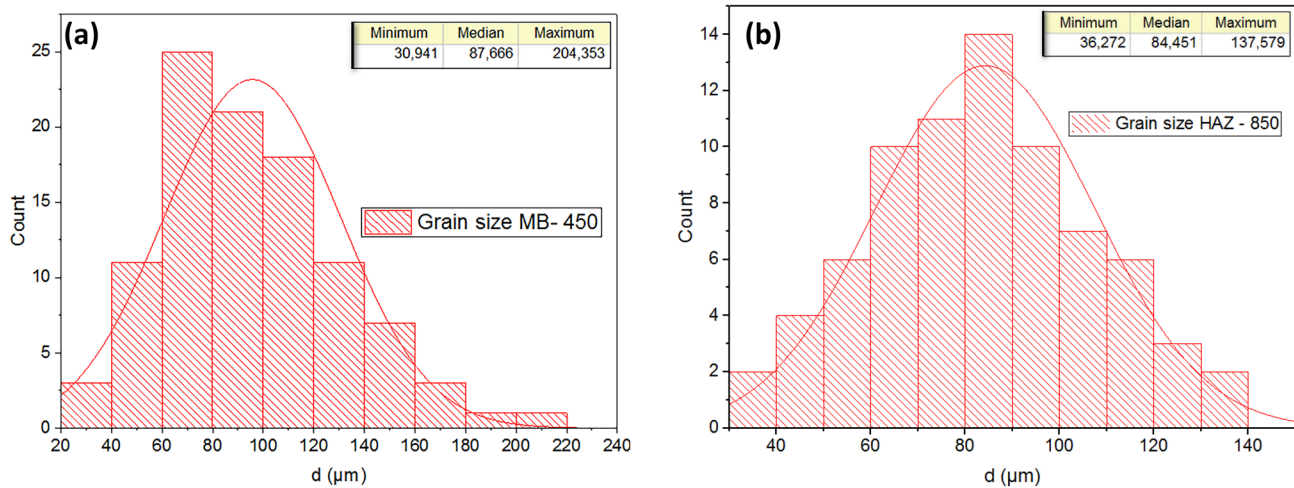
Fig. 6 Typical estimate of the grains size for all weldments in **a** BM and **b** HAZ

the HAZ increases with a polyhedral shape and a typical twinning [26–28]. Figure 6 shows a typical estimate of the grains size of the BM and the HAZ for different samples, as summarized in the Table 3. At PWHT of 450 °C, the microstructure of the BM becomes coarse (87.66 µm on average), but retains the same shape as the as-welded specimen which proves a grain size about 81.92 µm. At 650 °C, the microstructure undergoes partial recrystallization, and becomes less coarse (83.94 µm) with decreasing of the twin crystals rate [3, 29, 30]. In the 850 °C heat treatment, the grains are similarly equiaxed. It can also be observed that the grains do not show significant growth compared to those obtained at 650 °C (84.29 µm), but still larger than those of the as-weld specimen with appearance of new small grains, characteristic of a recrystallization mechanism. The size of the austenite grains in the HAZ has been reduced enclosed between 84.45 and 95.98 µm compared to the as-weld specimen (102.95 µm). This can be attributed to fast cooling during water quenching [12, 14, 31]. Finally at 1050 °C, there is an increase in the austenitic grains size of the BM (93.30 µm) and HAZ (108.53 µm) with a high rate of twins [30, 31].

Figure 7 presents the microstructure of the welded metals obtained from different specimens. It has a dendritic

aspect of solidification; the austenite matrix (γ) contains delta ferrite dendrites (δ) characterized by a skeletal morphology [7, 12, 13, 32]. The microstructures of the weld metal heat-treated at 450–1050 °C are similar to the as-weld microstructure; however, different dendrite shapes and sizes can be observed. The formation of a structure under a given morphology during solidification is determined by the G/R ratio (G is the temperature gradient and R is the cooling rate) [13]. Since the cooling conditions of the heat treated samples are the same, the only parameter affecting the microstructure is the temperature gradient. Cellular growth structures form rather than dendritic structure if G/R ratio is high [33–36]. In this respect, the morphological transition to the cell shape is expected in terms of interface evolution theory (the high temperature gradient can stabilize the solidification interface). The phase boundary between austenite and delta ferrite is considered to migrate in favor of decreasing interfacial energy [14, 33]. The skeletal type delta ferrite changed from (columnar + equiaxed) to cellular type by progression during heat treatment. The columnar morphology is attributed to the fast cooling on the base metal side. Consequently, the columnar form is the predominant type [36, 37], knowing that at 450 °C, it becomes (equiaxed + columnar), then purely equiaxed at 650 °C, and at 850 °C, it stabilizes at a finer equiaxed, and finally at 1050 °C, it is characterized by a cellular dendritic. As-welded delta ferrite dendrites were initially thin, and becomes thicker during heat treatment without losing their total volume fraction (34%) [8, 14, 21, 38].

Table 3 Grains size of BM and HAZ for all specimens

Specimen	Grains size BM (µm)	Grains size HAZ (µm)
As-welded	81.92	102.95
450 °C	87.66	95.98
650 °C	83.94	95.73
850 °C	84.29	84.45
1050 °C	93.30	108.53

Table 4 Width of delta ferrite dendrites δ in the WZ for all specimens

Specimen	As-welded	450 °C	650 °C	850 °C	1050 °C
Width (µm)	3.01	3.31	3.62	4.04	4.36

Fig. 7 Optical and SEM micrographs of the weld zone for all weldments: **a**, **b** as-welded, **c**, **d** PWHT at 450 °C, **e**, **f** PWHT at 650 °C, **g**, **h** PWHT at 850 °C, **i**, **j** PWHT at 1050 °C
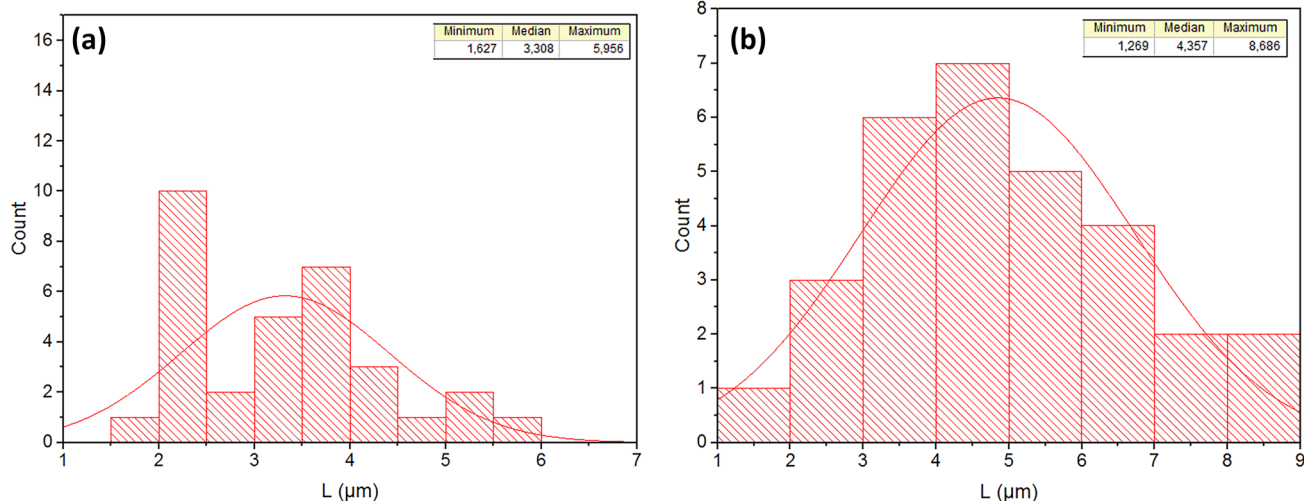
Fig. 8 Typical estimate of average width of delta ferrite dendrites δ in the WZ for all weld specimens: **a** PWHT at 450 °C, **b** PWHT at 1050 °C

Figure 8 shows a typical estimate of the average width of delta ferrite dendrites δ in the WZ for all specimens, which are summarized in Table 4.

3.3 XRD and EDS analysis

Figure 9 presents the results of the X-ray diffraction test in the base metal and weld zone for all samples. As can be observed, XRD diffractograms only confirmed the presence of austenite, whereas ferrite and chromium carbide or σ phases were not observed. EDS line test was performed since XRD test could not detect phases such as σ phase or chromium carbide in the phase percentages of less than 5% [14, 22, 25]. Figure 10 shows the results related to EDS line in the different zone of weldments. As can be seen in Fig. 10, there was no unusual accumulation of elements along the line, suggesting the absence of formation intermetallic compounds. Based on the chemical composition of the materials, base metal 304, and filler metal ER308Si, Cr, Ni, and Mo amounts were no increased and the amount of Fe was not reduced along the fusion line. As a result, the formation of chromium carbide at the interface was not observed.

When the austenitic stainless steel is maintained at temperatures between 500 and 900 °C, precipitation of chromium carbides occurs at the grain boundaries. And during welding, the heat affected zone HAZ, which has reached the temperature range of 550–850 °C, is the area most susceptible to such precipitates. Also, time is an essential parameter contributing to chromium carbide precipitation, as shown in Fig. 11. The chromium carbide could be dissolved in heat treatment between 1040 and 1150 °C, and go into solid solution [31, 39]. To avoid chromium carbide formation in the critical temperature range, the cooling must be rapid [7, 22, 40]. For this reason, the sample treated at
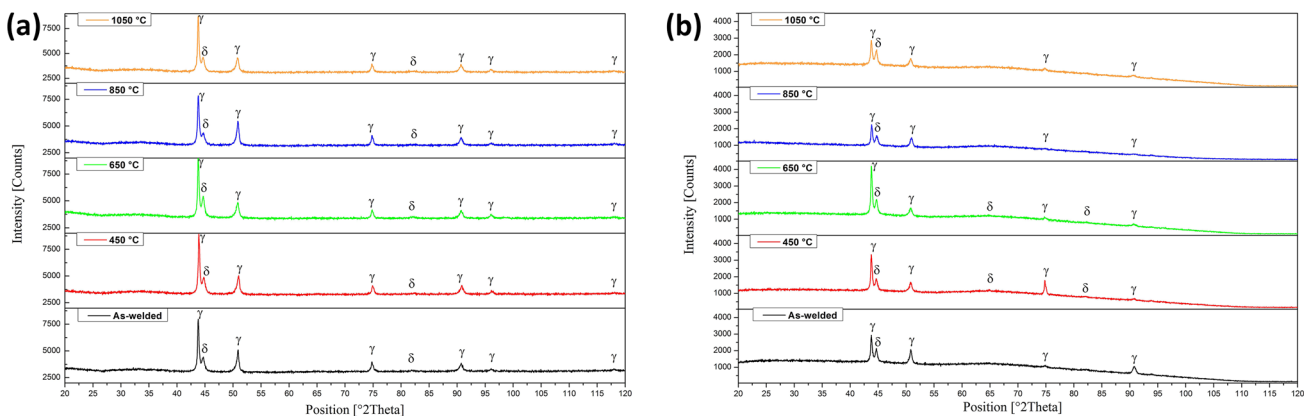

Fig. 9 X-ray diffraction difractograms of the all weldments in the **a** base metal BM and **b** weld zone WZ
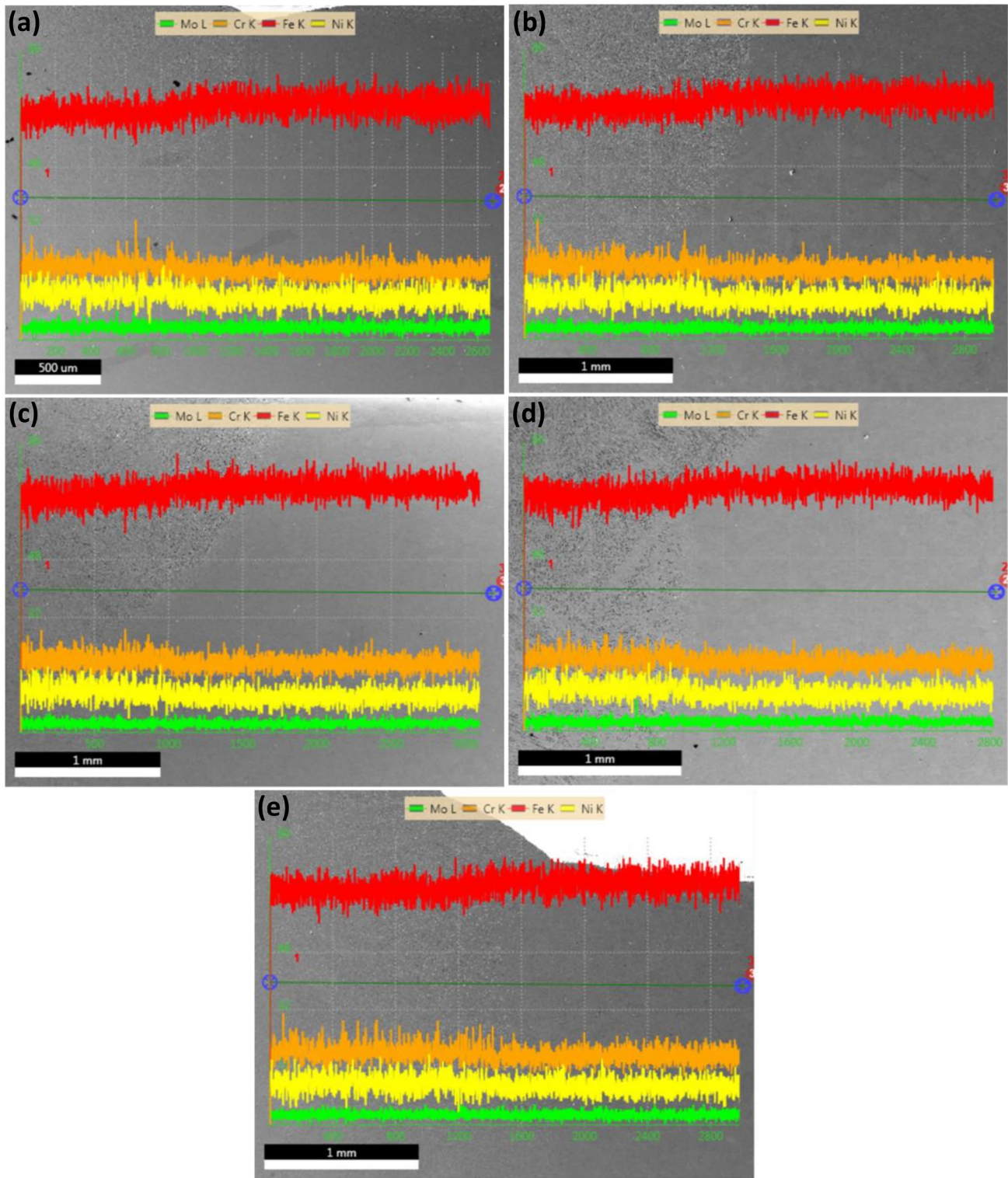
Fig. 10 Elements scanning result on the weld fusion line in **a** as-welded, **b** PWHT at 450 °C, **c** PWHT at 650 °C, **d** PWHT at 850 °C, **e** PWHT at 1050 °C
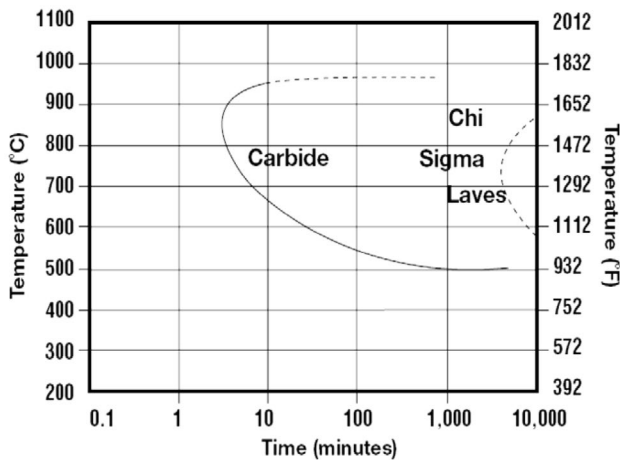
Fig. 11 Isothermal precipitation diagram for 304 austenitic stainless steel [7, 22, 40]

a temperature of 1050 °C did not show any precipitation. To confirm the above assumptions, EDS analysis in the HAZ was performed for the different weldments (Fig. 12). We observe the absence of precipitates and the presence of traces of manganese oxide in the as welded and PWHT at 1050 °C samples.

3.4 Mechanical properties

3.4.1 Tensile testing

It can be clearly seen that the tensile fractures of the five specimens are located at the base metal as shown in the fracture path of Fig. 13. This demonstrated that welding conditions and heat treatment temperatures applied to all specimens were appropriate.

Figure 14 illustrates the stress–strain curves of the as-welded and PWHT joints. The detailed values of yield strength and ultimate tensile strength are summarized in Table 5. The results show that the highest tensile strength value were those recorded for the as-welded specimen with a maximum ultimate tensile strength of 672.4 MPa and a maximum yield strength of 290 MPa. Moreover, the tensile and yield values of the PWHT specimens are very close, which proves that the PWHT temperature has low impact on tensile strengths. On the other hand, with increasing PWHT temperatures, the elongation of the specimens improved in particular at 450 and 650 °C, the values 19.027% and 20.713% are recorded respectively which is due to reduction

of the residual stress and twin crystals rate in the specimens except at 850 °C where a lower value is recorded due to the more particular structural changes of the HAZ and the base metal, which becomes fine equiaxed [39]. Finally, the specimens at 1050 °C showed lower tensile strength than the as-weld specimen, and an elongation close to that of heat-treated specimens [14]. We can conclude that these changes in mechanical behavior can be proved based on the micro-structural changes during heat treatment [41].

SEM micrographs of the fracture surfaces of all specimens show ductile fracture with fine and coarse dimples (Fig. 15) [39, 42]. The as-weld fracture surface shows small dimples usually surrounded by large and deep ones. At 450 °C, it includes a combination of deep and wide dimples. At 650 °C, it consists of fine and uniform dimples, which indicates a strong plasticity. At 850 °C, dimples become larger and shallower, indicating that the plasticity of the joint becomes poorer, which is consistent with the elongation results [16, 43]. Also, it can be seen that the number of micro-voids increased. Compared to the as-weld fracture, dimples in the joint heat treated at 1050 °C are of medium sizes and shallow with some large dimples [13].

3.4.2 Micro-hardness testing

The micro-hardness profiles of the five specimens are illustrated in Fig. 16. Clearly, all the weld zones (WZs) exhibited lower micro-hardness values (about 135–165 HV) relative to the base metal BM and heat affected zone HAZ. This is due to the high delta ferrite content in the weld zone [14, 44]. In addition, it is clearly observed that the micro-hardness value of the weld metal compared to the as-welded samples decreases up to a heat treatment temperature of 650 °C and increases starting from 850 °C [14]. The HAZ presents similar micro-hardness values for all samples and slightly higher than that of the base metal except for the weld heat treated at 850 °C. The latter exhibits high micro-hardness values (about 210 HV) due to the accordance of the grain refinement. The sample heat treated at 1050 °C presents the best and stable micro-hardness profile similar to that of the as-weld specimen but with high values in the weld zone. It was also found that the heat treated weldment at 650 °C showed the highest micro-hardness of base metal (about 190 HV) due to the high content of twins [41, 44]. According to the micro-hardness profile, it is confirmed that the rupture of all tensile specimens appeared at the level of HAZ except for the specimen heat treated at 650 °C which presented a rupture in the BM.
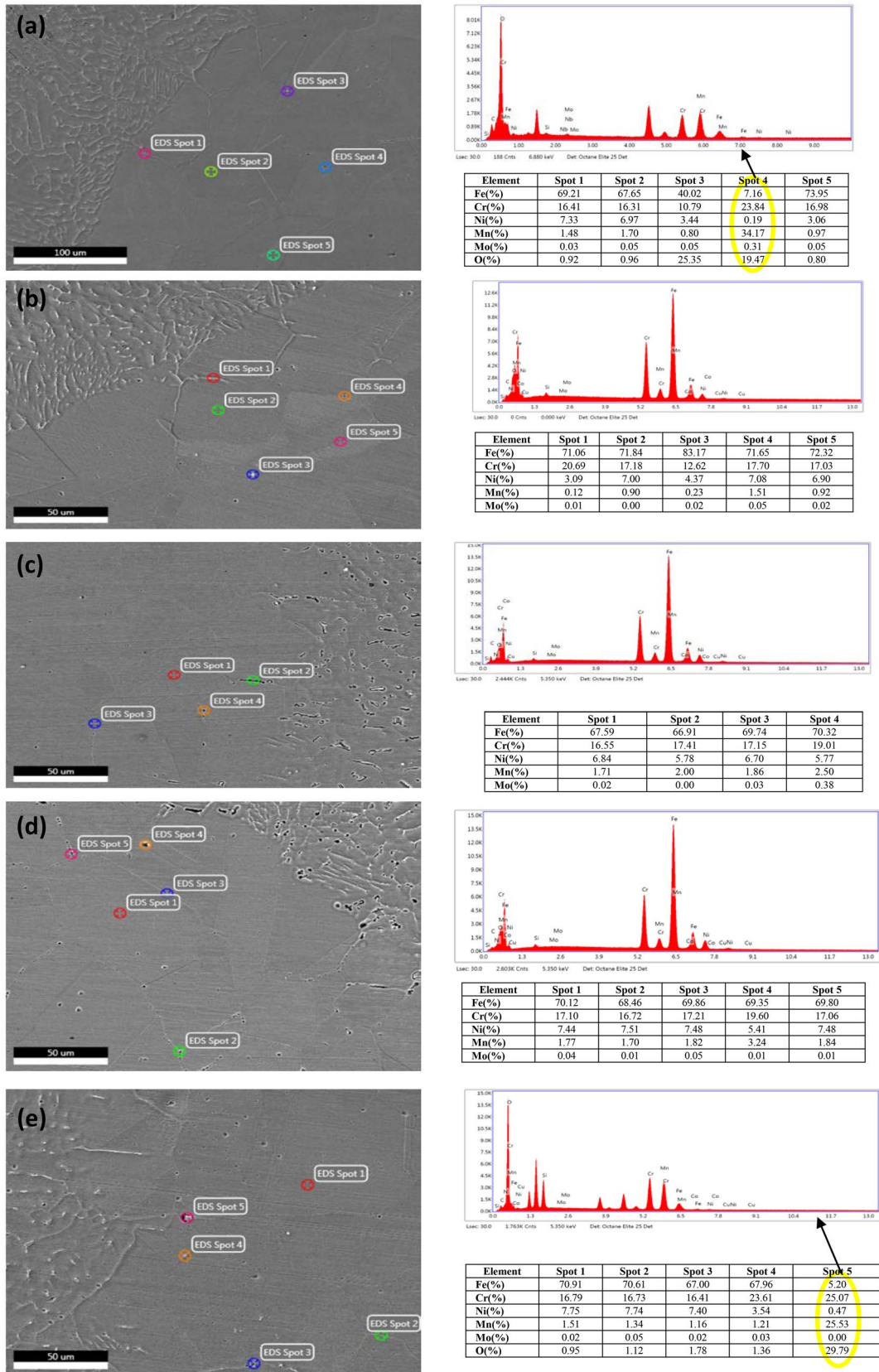
Fig. 12 Elements line scanning result of weldments in **a** as-welded, **b** PWHT at 450 °C, **c** PWHT at 650 °C, **d** PWHT at 850 °C, **e** PWHT at 1050 °C

Fig. 13 Tensile tested samples in as-received and various heat treatment conditions
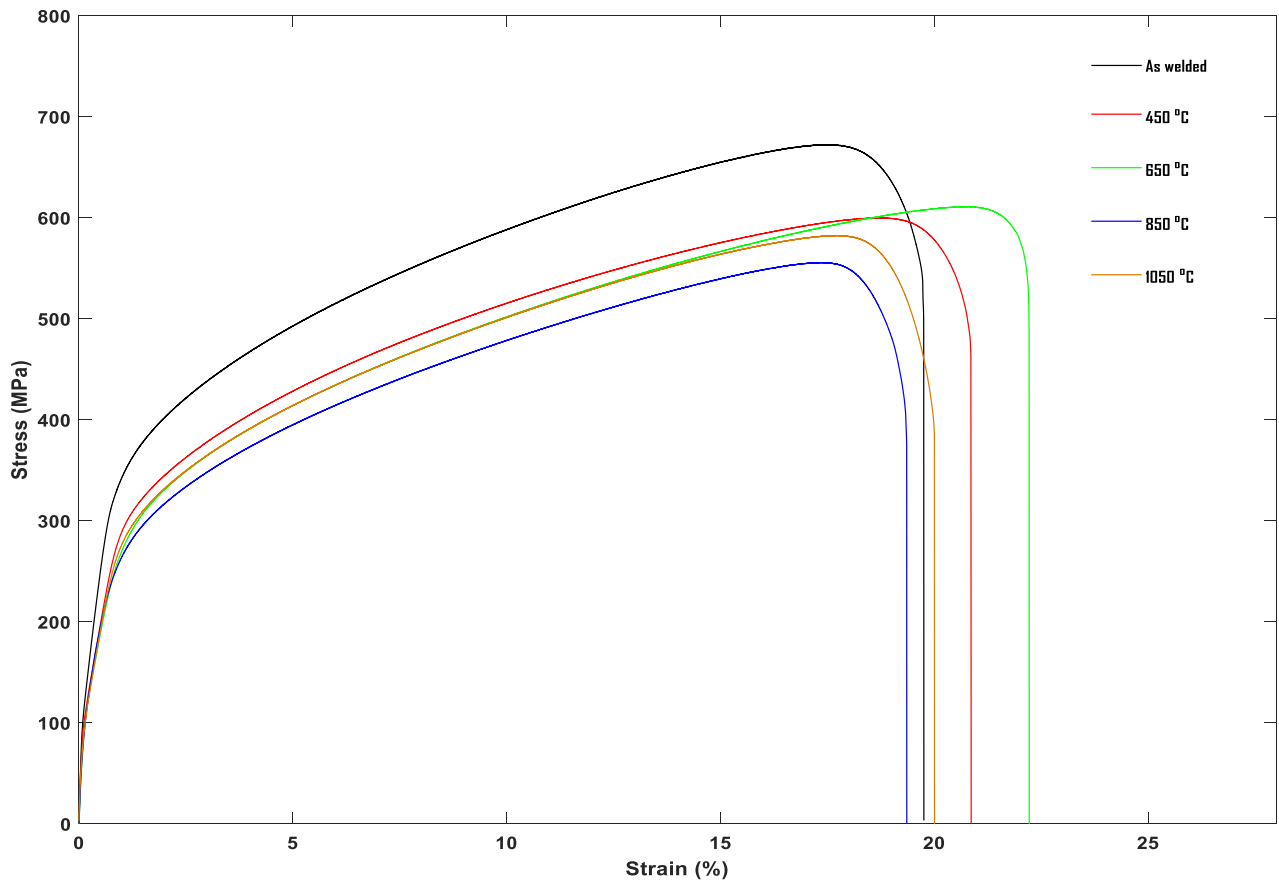

Fig. 14 The result of strength test for the as-welded and heat treated specimens

Table 5 Tensile properties of as welded and heat treated specimens

Specimen	Ultimate tensile strength (MPa)	Yield strength 0.2% (MPa)	Elongation (%)
As-welded	672.4	290	17.526
450 °C	599.9	284	19.027
650 °C	610.9	250	20.713
850 °C	555.6	225	17.409
1050 °C	582.4	260	17.767

Fig. 15 SEM micrograph of the tensile fractured of the specimens: **a** as-welded, **b** PWHT at 450 °C, **c** PWHT at 650 °C, **d** PWHT at 850 °C, **e** PWHT at 1050 °C
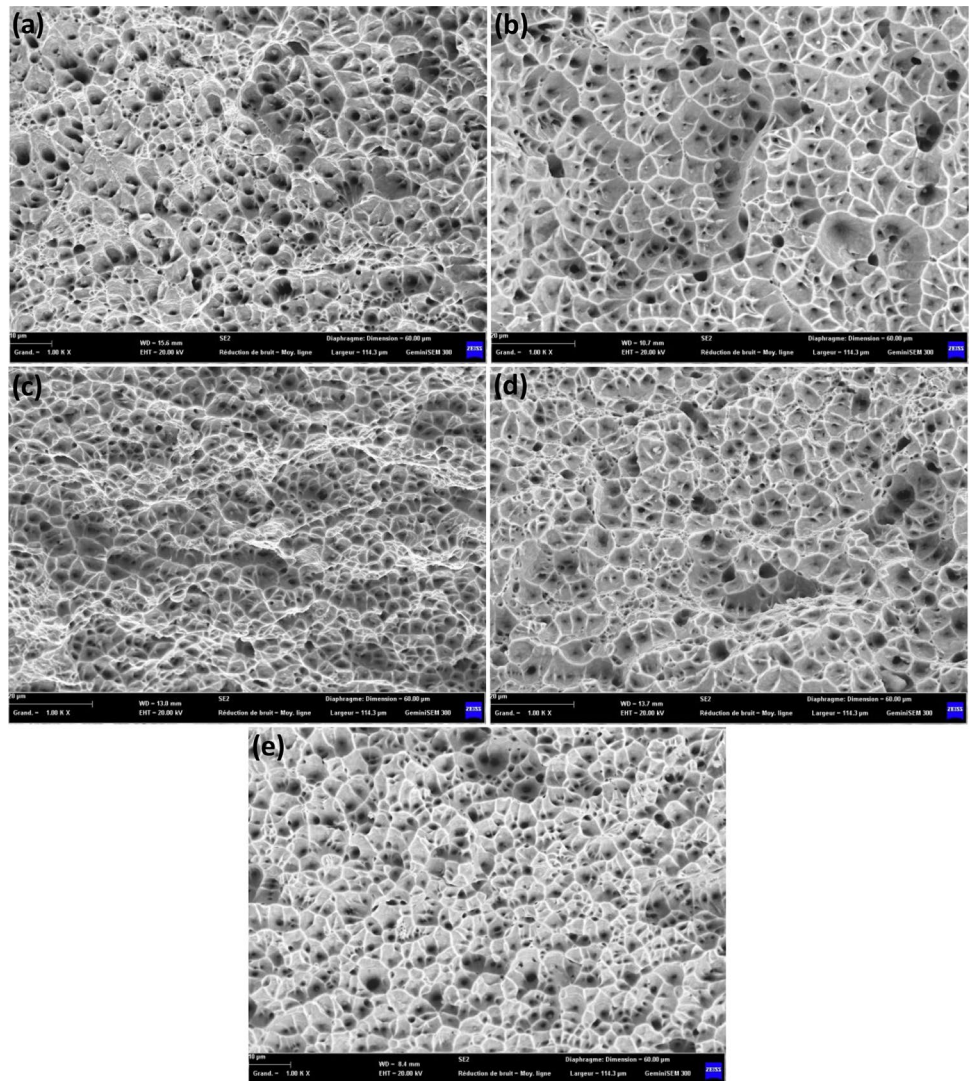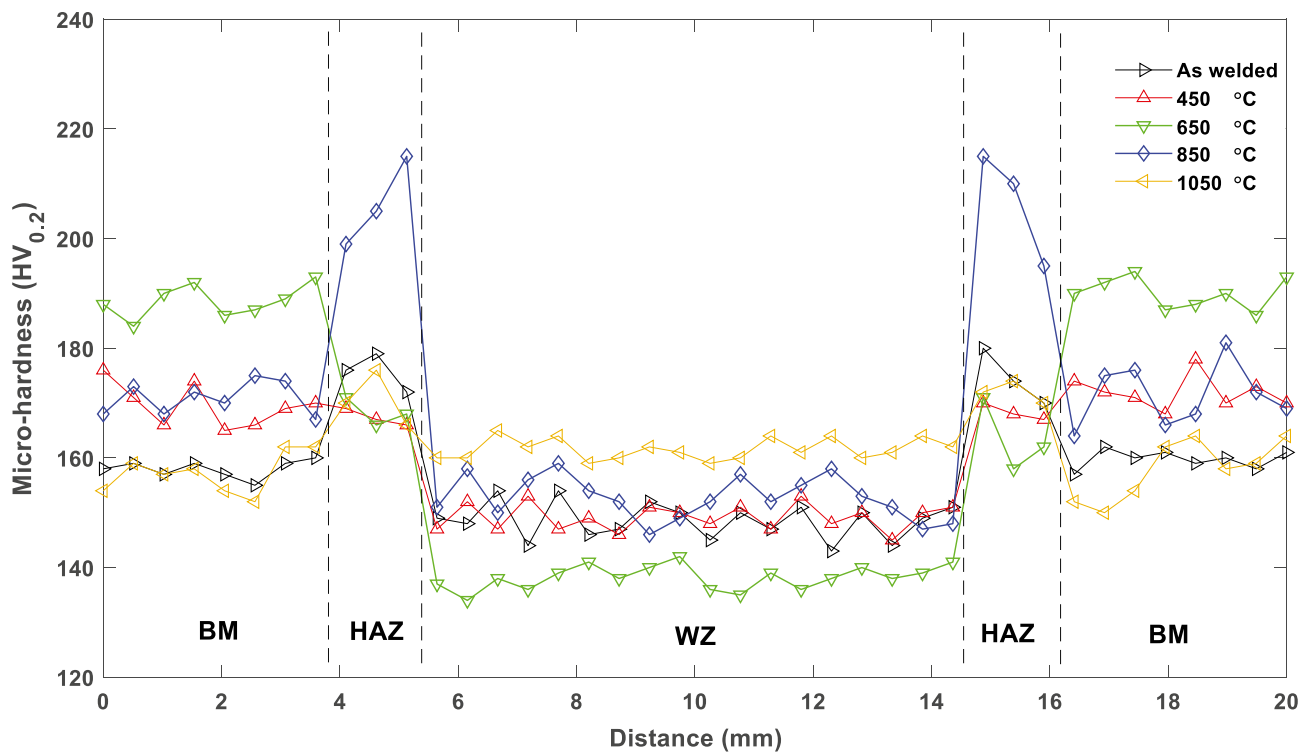
Fig. 16 Micro-hardness profile across the as-welded and heat treated specimens

4 Conclusion

On the basis of present work, the major outcomes are given below:

(1) The BM grains size increased, and the twin crystals rate decreased with increasing heat treatment temperature up to 850 °C. At this later, the grains are similarly equiaxed with appearance of new small grains. The size of the austenite grains is enclosed between 83.94 and 87.66 μm, which is not much modified compared to the as-welded sample (81.92 μm). However, at 1050 °C, there is a significant increase in the austenitic grains size (93.30 μm).

(2) The HAZ grains size decreased with increasing heat treatment temperature up to 850 °C (84.45–95.98 μm) compared to the as-welded sample (102.95 μm). However, at 1050 °C, there is an increase in the austenitic grains size (108.53 μm).

(3) X-ray diffraction and energy-dispersive spectroscopy techniques revealed the non-existence of intermetallic phases as σ or chromium carbide.

(4) The PWHT temperature has low impact on the tensile strengths but improves the elongation of the weld-ments. This can clearly be seen for the specimen treated at 650 °C, and which shows a better ductility.

(5) The micro-hardness for all the weld zones (WZs) exhibited lower values compared to the base metal (BM) and heat affected zone (HAZ).

(6) The PWHT at 1050 °C presents the best and stable micro-hardness profile, similar to that of the as-weld specimen but with higher values in the weld zone. Otherwise, the PWHT at 650 and 850 °C should be avoided due to the non-homogeneous micro-hardness profile.

(7) Based upon the present study, it is suggested that the microstructural changes always play a significant role in determining the mechanical properties of the weldment and can be improved by varying the temperature or time of the post-weld heat treatment.

Declarations

Ethics approval Not applicable.

Consent to participate Not applicable.

Consent for publication The authors give all the rights to publish the material presented in this work.

Competing interests The authors declare no competing interests.

References

1. Cunat PJ (2000) Aciers inoxydables - Critères de choix et structure. Techniques de l'Ingénieur, traité Matériaux métalliques M4(540):4–10

2. Moteshakker A, Danaee I, Moeinifar S, Ashrafi A (2015) Hardness and tensile properties of dissimilar welds joints between SAF 2205 and AISI 316L. Sci Technol Weld Joining 21(1):1–10. https://doi.org/10.1179/1362171815Y.0000000062

3. Jang D, Kim K, Kim HC, Jeon JB, Nam DG, Sohn KY, Kim BJ (2017) Evaluation of mechanical property for welded austenitic stainless steel 304 by Following Post Weld Heat Treatment. Korean J Met Mater 55(9):664–670. https://doi.org/10.3365/KJMM.2017.55.9.664

4. Kellai A, Kahla S, Dehimi S, Babes B (2021) Microstructural and mechanical properties of welding and thermal spraying coatings on ductile cast iron. J Defect Diffus Forum 406:300–311. https://doi.org/10.4028/www.scientific.net/DDF.406.300

5. Moslemi N, Redzuan N, Ahmad N, Hor TR (2015) Effect of current on characteristic for 316 stainless steel welded joint including microstructure and mechanical properties. Procedia CIRP 26:560–564. https://doi.org/10.1016/j.procir.2015.01.010

6. Amudarasan NV, Palanikumar K, Shanmugam K (2014) Mechanical properties of AISI 316L austenitic stainless steels welded by GTAW. Adv Mater Res 849:50–57. https://doi.org/10.4028/www.scientific.net/AMR.849.50

7. Silva CC, Farias JP, de Sant'Ana HB (2009) Evaluation of AISI 316L stainless steel welded plates in heavy petroleum environment. Mater Des 30:1581–1587. https://doi.org/10.1016/j.matdes.2008.07.050

8. Yan J, Gao M, Zeng X (2010) Study on microstructure and mechanical properties of 304 stainless steel joints by TIG, laser and laser-TIG hybrid welding. Opt Lasers Eng 48:512–517. https://doi.org/10.1016/j.optlaseng.2009.08.009

9. Dadfar M, Fathi MH, Karimzadeh F, Dadfar MR, Saatchi A (2007) Effect of TIG welding on corrosion behavior of 316L stainless steel. Mater Lett 61:2343–2346. https://doi.org/10.1016/j.matlet.2006.09.008

10. Fei Z, Cuiuri D, Li H, Huang W, Peng Z (2020) Effect of post-weld heat treatment on microstructure and mechanical properties of deep penetration autogenous TIG-welded dissimilar joint between creep strength enhanced ferritic steel and austenitic stainless steel. Int J Adv Manuf Technol 108:3207–3229. https://doi.org/10.1007/s00170-020-05605-2

11. Jamshidi Aval H, Farzadi A, Serajzadeh S, Kokabi AH (2008) Theoretical and experimental study of microstructures and weld pool geometry during GTAW of 304 stainless steel. Int J Adv Manuf Technol 42(11):1043–1051. https://doi.org/10.1007/s00170-008-1663-6

12. Barbosa Goncalvesa R, de Araujoa PHD, Bragab FJV, Terronesc LAH, da Rocha Paranhos RP (2016) Effect of conventional and alternative solution and stabilizing heat treatment on the microstructure of a 347 stainless steel welded joint. Weld Int 31:196–205. https://doi.org/10.1080/09507116.2016.1218625

13. Safari M, Mostaan H, Derakhshan E (2018) Microstructual and mechanical studies of the dissimilar tabular joints of Incoloy alloy 825 and AISI 316 stainless steel. J Mar Eng Technol 19(4):176–185. https://doi.org/10.1080/20464177.2018.1508805

14. Nam T, An E, Kim BJ, Shin S, Ko WS, Park N, Kang N, Jeon JB (2018) Effect of post weld heat treatment on the microstructure and mechanical properties of a submerged-arc-welded 304 stainless steel. Metals 8(26):1–13. https://doi.org/10.3390/met8010026

15. Sassoulas H (1997) Aciers inoxydables. Partie 1. Liste des aciers inoxydables. Traitements thermiques des aciers inoxydables. Traitement des metaux M1 155–2, pp 2–14

16. Xin J, Fang C, Song Y, Wei J, Xu S, Wu J (2017) Effect of post weld heat treatment on the microstructure and mechanical properties of ITER-grade 316LN austenitic stainless steel weldments. Cryogenics 83:1–7. https://doi.org/10.1016/j.cryogenics.2017.02.001

17. Erdem M, Altuğ M, Karabulut M (2016) Investigation of mechanical, microstructural, and machining properties of AISI 420 martensitic stainless steel welded by laser welding. Int J Adv Manuf Technol 85:481–492. https://doi.org/10.1007/s00170-015-7924-2

18. Kožuh S, Gojić M, Kosec L (2007) The effect of annealing on properties of AISI 316L base and weld metals. Mater Geoenviron 54(3):331

19. ASTM E8–04 (2008) Standard test methods for tension testing of metallic materials

20. Terada M, Saiki M, Costa I et al (2006) Microstructure and intergranular corrosion of the austenitic stainless steel 1.4970. J Nucl Mater 358:40–46. https://doi.org/10.1016/j.jnucmat.2006.06.010

21. Ghadam Dezfuli MA, Dehmolaei R, Alavi Zaree SR (2019) Microstructural aspects of 304 stainless steel weld joints with the simultaneous application of electromagnetic vibration. Metallogr Microstruct Anal 8:226–232. https://doi.org/10.1007/s13632-019-00521-8

22. Khodadadi A, Shamanian M, Karimzadeh F (2017) Microstructure and mechanical properties of dissimilar friction stir spot welding between St37 steel and 304 stainless steel. J Mater Eng Perform 26(6):2847–2858. https://doi.org/10.1007/s11665-017-2703-x

23. Das D, Pratihar DK, Roy GG (2018) Cooling rate predictions and its correlation with grain characteristics during electron beam welding of stainless steel. Int J Adv Manuf Technol 97(5):2241–2254. https://doi.org/10.1007/s00170-018-2095-6

24. Wu C, Li S, Zhang C, Wang X (2016) Microstructural evolution in 316LN austenitic stainless steel during solidification process under different cooling rates. J Mater Sci 51(5):2529–2539. https://doi.org/10.1007/s10853-015-9565-0

25. Kumar P, Sinha AN, Hirwani CK, Murugan M, Saravanan A, Singh AK (2021) Effect of welding current in TIG welding 304L steel on temperature distribution, microstructure and mechanical properties. J Braz Soc Mech Sci 43(7):1–20. https://doi.org/10.1007/s40430-021-03082-6

26. Vashishtha H, Taiwade RV, Sharma S, Patil AP (2017) Effect of welding processes on microstructural and mechanicalproperties of dissimilar weldments between conventional austeniticand high nitrogen austenitic stainless steels. J Manuf Process 25:49–59. https://doi.org/10.1016/j.jmapro.2016.10.008

27. Basyigit AB, Murat MG (2018) The effects of TIG welding rod compositions on microstructural and mechanical properties of dissimilar AISI 304L and 420 Stainless Steel Welds. Metals 8(11):1–14. https://doi.org/10.3390/met8110972

28. Dománková M, Kocsisová E, Slatkovský I, Pinke P (2014) The microstructure evolution and its effect on corrosion properties of 18Cr-12Ni-2,5Mo steel annealed at 500–900°C. Acta Polytech Hung 11(3):125–137. https://doi.org/10.12700/APH.11.03.2014.03.8

29. Liu GL, Yang SW, Han WT, Zhou LJ, Zhang MQ, Ding JW, Misra RDK (2018) Microstructural evolution of dissimilar welded joints between reduced-activation ferritic-martensitic steel and 316L stainless steel during the post weld heat treatment. Mater Sci Eng A 722:182–196. https://doi.org/10.1016/j.msea.2018.03.035

30. Dak G, Pandey C (2021) Experimental investigation on micro-structure, mechanical properties, and residual stresses of dissimilar welded joint of martensitic P92 and AISI 304L austenitic stainless steel. Int J Press Vessels Pip 194:104536. https://doi.org/10.1016/j.ijpvp.2021.104536

31. Abioye TE, Omotehinse IS, Oladele IO, Olugbade TO, Ogedengbe TI (2020) Effects of post-weld heat treatments on the microstructure, mechanical and corrosion properties of gas metal arc welded 304 stainless steel. World J Eng 17(1):87–96. https://doi.org/10.1108/WJE-11-2019-0323

32. Kangazian J, Shamanian M (2016) Multiresponse optimization of pulsed-current gas tungsten arc welding (PCGTAW) for AISI 304 stainless steel to St 52 steel dissimilar welds. Metallogr Microstruct Anal 5:1–10. https://doi.org/10.1007/s13632-016-0277-x

33. Fu JW, Yang YS, Guo JJ, Tong WH (2008) Effect of cooling rate on solidification microstructures in AISI 304 stainless steel. Mater Sci Eng 24(8):941–944. https://doi.org/10.1179/174328408X295962

34. Hao Y, Li J, Li X, Liu W, Cao G, Li C, Liu Z (2020) Influences of cooling rates on solidification and segregation characteristics of Fe-Cr-Ni-Mo-N super austenitic stainless steel. J Mater Process Technol 275:116326. https://doi.org/10.1016/j.jmatprotec.2019.116326

35. Fukumoto S, Fujiwara K, Toji S, Yamamoto A (2008) Small-scale resistance spot welding of austenitic stainless steels. Mater Sci Eng A 492(1–2):243–249. https://doi.org/10.1016/j.msea.2008.05.002

36. Ventrella VA, Berretta JR, De Rossi W (2010) Pulsed Nd: YAG laser seam welding of AISI 316L stainless steel thin foils. J Mater Process Technol 210(14):1838–1843. https://doi.org/10.1016/j.jmatprotec.2010.06.015

37. Katayama S, Matsunawa A (1984) Solidification microstructure of laser welded stainless steels. Int Congress Appl Lasers Electro-Optics 1984(2):(60–67). Laser Institute of America. https://doi.org/10.2351/1.5057623

38. Sharma S, Taiwade RV, Yadav A, Vashishtha H (2019) Influence of fillers and welding processes on the microstructural evolution, mechanical properties and corrosion behavior of dissimilar Hastelloy C-22/AISI 321 joints. Mater Res Express 6:1–14. https://doi.org/10.1088/2053-1591/ab316b

39. Aghayar Y, Naghashzadeh A, Atapour M (2021) An assessment of microstructure and mechanical properties of inconel 601/304 stainless steel dissimilar weld. Vacuum 184:1–10. https://doi.org/10.1016/j.vacuum.2020.109970

40. Weiss B, Stickler R (1972) Phase instabilities during high temperature exposure of 316 austenitic stainless steel. Metall Mater Trans B 3(4):851–866. https://doi.org/10.1007/BF02647659

41. Yang J, Wang Y, Li F, Huanga W, Jing G, Wang Z, Zeng X (2019) Weldability, microstructure and mechanical properties of laser-welded selective laser melted 304 stainless steel joints. J Mater Sci Technol 35:1817–1824. https://doi.org/10.1016/j.jmst.2019.04.017

42. Kellai A, Lounis A, Kahla S, Idir B (2018) Effect of root pass filler metal on microstructure and mechanical properties in the multi-pass welding of duplex stainless steels. Int J Adv Manuf Technol 95:3215–3225. https://doi.org/10.1007/s00170-017-1412-9

43. Wang H, Wang K, Wang W, Huang L, Peng P, Yu H (2019) Microstructure and mechanical properties of dissimilar friction stir welded type 304 austenitic stainless steel to Q235 low carbon steel. Mater Charact 155:1–12. https://doi.org/10.1016/j.matchar.2019.109803

44. Chuaiphan W, Srijaroenpramong L (2014) Effect of welding speed on microstructures, mechanical properties and corrosion behaviour of GTA-welded AISI 201 stainless steel sheets. J Mater Process Technol 214:402–408. https://doi.org/10.1016/j.jmatprotec.2013.09.025